Electronic Supplementary Information

Prediction of Boridenes as High Performance Anodes for Alkaline Metal

and Alkaline Earth Metal Ion Batteries

Baiyi Chen[a], Haoliang Liu[a], Tianyu Bai[a], Zifeng Song[a], Jin'an Xie[a], Kai Wu[a], Yonghong Cheng[a] and Bing Xiao[a]*

[a]. State Key Laboratory of Electrical Insulation and Power Equipment, School of

Electrical Engineering, Xi'an Jiaotong University, Xi'an 710049, China

Corresponding author: bingxiao84@xjtu.edu.cn

calculation formula

Calculate the open circuit voltage (OCV), and the change of Gibbs free energy of the half-cell reaction can be obtained from the formula S(1).

$$\Delta G = \Delta E + P\Delta V - T\Delta S \qquad\qquad S(1)$$

Where ΔG is the change of Gibbs free energy.

ΔE is the change of energy in the system.

$P\Delta V$ is the energy change caused by the change of volume and pressure of the system.

$T\Delta S$ is the energy change caused by the change of temperature and entropy of the system.

At room temperature, $P\Delta V$ and $T\Delta S$ are 10^{-5} eV and 26 meV, respectively, which are much smaller than the internal energy change ΔE of the system. Therefore, the contribution of both can be ignored in the calculation, so the change of Gibbs free energy of the system is equal to the differential adsorption energy in the adsorption process.

Table S1: Adsorption energies and Bader charge analysis of a single surface group absorbed at different adsorption sites for $Mo_{3/4}B_2T_{1/12}$ Boridenes.

$Mo_{16}B_{24}T_1$	Hollow				Bridge				Top			
	DAE	Bader charge (e⁻)			DAE	Bader charge (e⁻)			DAE	Bader charge (e⁻)		
	(eV)	Mo	B	T	(eV)	Mo	B	T	(eV)	Mo	B	T
O	Relaxed to Bridge				-6.10	-0.51	0.30	0.97	-5.35	-0.50	0.30	0.85
OH	Relaxed to Bridge				-5.95	-0.49	0.30	0.59	-5.50	-0.48	0.30	0.53
F	-3.25	-0.49	0.29	0.80	-5.52	-0.48	0.29	0.69	-5.27	-0.49	0.29	0.65

Table S2: Thermodynamic reaction equations and formation enthalpies of alkaline (earth) metal adsorbate on $Mo_{3/4}B_2O_2$ Boridenes.

metal	reaction equation	formation enthalpy (eV)
Li	$\frac{1}{4}Mo_{4/3}B_2O_2 + Li = \frac{1}{4}Mo_{4/3}B_2 + \frac{1}{2}Li_2O$	-1.30
Na	$\frac{1}{4}Mo_{4/3}B_2O_2 + Na = \frac{1}{4}Mo_{4/3}B_2 + \frac{1}{2}Na_2O$	-0.47
K	$\frac{1}{4}Mo_{4/3}B_2O_2 + K = \frac{1}{4}Mo_{4/3}B_2 + \frac{1}{2}K_2O$	-0.03
Mg	$\frac{1}{2}Mo_{4/3}B_2O_2 + Mg = \frac{1}{2}Mo_{4/3}B_2 + MgO$	-2.68
Ca	$\frac{1}{2}Mo_{4/3}B_2O_2 + Ca = \frac{1}{2}Mo_{4/3}B_2 + CaO$	-3.13

Table S3: Thermodynamic reaction equations and formation enthalpies of alkaline (earth) metal adsorbate on $Mo_{3/4}B_2(OH)_2$ Boridenes.

metal	reaction equation	formation enthalpy (eV)

metal	reaction equation	formation enthalpy (eV)
Li	$\frac{1}{2}Mo_{4/3}B_2(OH)_2 + Li = \frac{1}{2}Mo_{4/3}B_2O_2Li_2 + \frac{1}{2}H_2$	-2.04
	$\frac{1}{2}Mo_{4/3}B_2O_2Li_2 + Li = \frac{1}{2}Mo_{4/3}B_2 + Li_2O$	-0.30
	$\frac{1}{4}Mo_{4/3}B_2(OH)_2 + Li = \frac{1}{4}Mo_{4/3}B_2 + \frac{1}{2}Li_2O + \frac{1}{4}H_2$	-1.17
	$\frac{1}{2}Mo_{4/3}B_2(OH)_2 + Li = \frac{1}{2}Mo_{4/3}B_2 + LiOH$	-1.09
Na	$\frac{1}{2}Mo_{4/3}B_2(OH)_2 + Na = \frac{1}{2}Mo_{4/3}B_2O_2Na_2 + \frac{1}{2}H_2$	-1.48
	$\frac{1}{2}Mo_{4/3}B_2O_2Na_2 + Na = \frac{1}{2}Mo_{4/3}B_2 + Na_2O$	0.79
	$\frac{1}{4}Mo_{4/3}B_2(OH)_2 + Na = \frac{1}{4}Mo_{4/3}B_2 + \frac{1}{2}Na_2O + \frac{1}{4}H_2$	-0.34
	$\frac{1}{2}Mo_{4/3}B_2(OH)_2 + Na = \frac{1}{2}Mo_{4/3}B_2 + NaOH$	-0.82
K	$\frac{1}{2}Mo_{4/3}B_2(OH)_2 + K = \frac{1}{2}Mo_{4/3}B_2O_2K_2 + \frac{1}{2}H_2$	-0.93
	$\frac{1}{2}Mo_{4/3}B_2O_2K_2 + K = \frac{1}{2}Mo_{4/3}B_2 + K_2O$	1.11
	$\frac{1}{4}Mo_{4/3}B_2(OH)_2 + K = \frac{1}{4}Mo_{4/3}B_2 + \frac{1}{2}K_2O + \frac{1}{4}H_2$	0.09
	$\frac{1}{2}Mo_{4/3}B_2(OH)_2 + K = \frac{1}{2}Mo_{4/3}B_2 + KOH$	-0.65
Mg	$Mo_{4/3}B_2(OH)_2 + Mg = Mo_{4/3}B_2O_2Mg + H_2$	-2.52
	$Mo_{4/3}B_2O_2Mg + Mg = Mo_{4/3}B_2 + 2MgO$	-2.33
	$\frac{1}{2}Mo_{4/3}B_2(OH)_2 + Mg = \frac{1}{2}Mo_{4/3}B_2 + MgO + \frac{1}{2}H_2$	-2.43
	$Mo_{4/3}B_2(OH)_2 + Mg = Mo_{4/3}B_2 + Mg(OH)_2$	-2.17
Ca	$Mo_{4/3}B_2(OH)_2 + Ca = Mo_{4/3}B_2O_2Ca + H_2$	-3.70
	$Mo_{4/3}B_2O_2Ca + Ca = Mo_{4/3}B_2 + 2CaO$	-2.06
	$\frac{1}{2}Mo_{4/3}B_2(OH)_2 + Ca = \frac{1}{2}Mo_{4/3}B_2 + CaO + \frac{1}{2}H_2$	-2.88
	$Mo_{4/3}B_2(OH)_2 + Ca = Mo_{4/3}B_2 + Ca(OH)_2$	-2.88

Table S4: Thermodynamic reaction equations and formation enthalpies of alkaline (earth) metal adsorbate on $Mo_{3/4}B_2F_2$ Boridenes.

metal	reaction equation	formation enthalpy (eV)
Li	$\frac{1}{2}Mo_{4/3}B_2F_2 + Li = \frac{1}{2}Mo_{4/3}B_2 + LiF$	-1.87
Na	$\frac{1}{2}Mo_{4/3}B_2F_2 + Na = \frac{1}{2}Mo_{4/3}B_2 + NaF$	-1.60

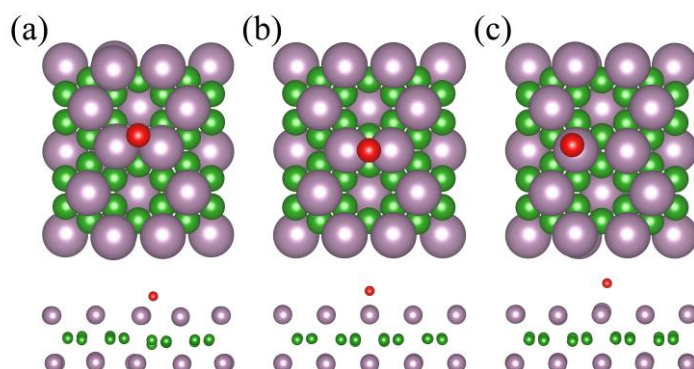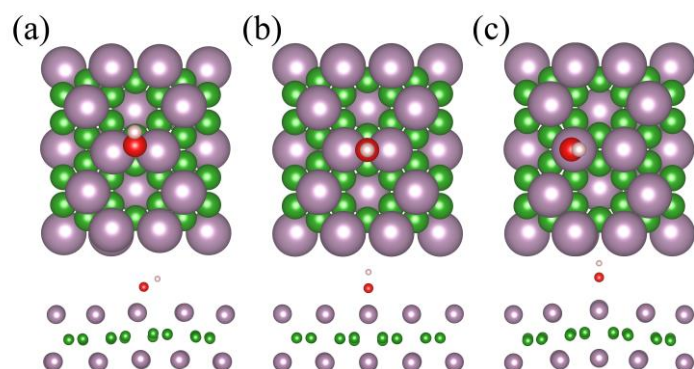|		
K	$\frac{1}{2}Mo_{4/3}B_2F_2 + K = \frac{1}{2}Mo_{4/3}B_2 + KF$	-1.32
Mg	$Mo_{4/3}B_2F_2 + Mg = Mo_{4/3}B_2 + MgF_2$	-2.55
Ca	$Mo_{4/3}B_2F_2 + Ca = Mo_{4/3}B_2 + CaF_2$	-3.87

Fig S1 Optimization results of O-termination adsorption sites: (a): hollow site; (b): bridge site and (c): top site.

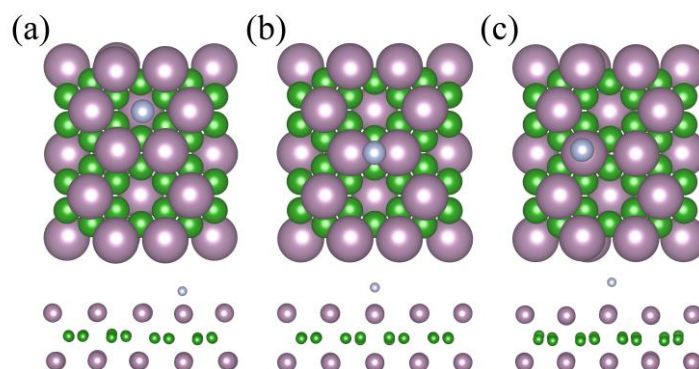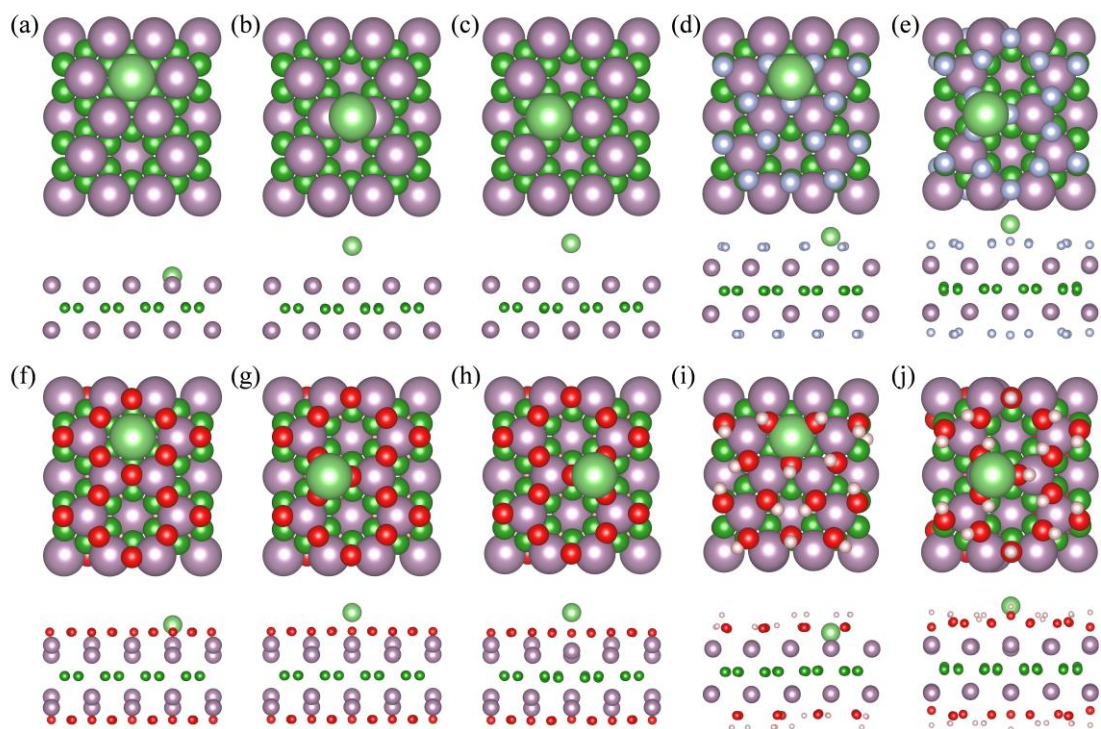Fig S2 Optimization results of OH-termination adsorption sites: (a): hollow site; (b): bridge site and (c): top site.

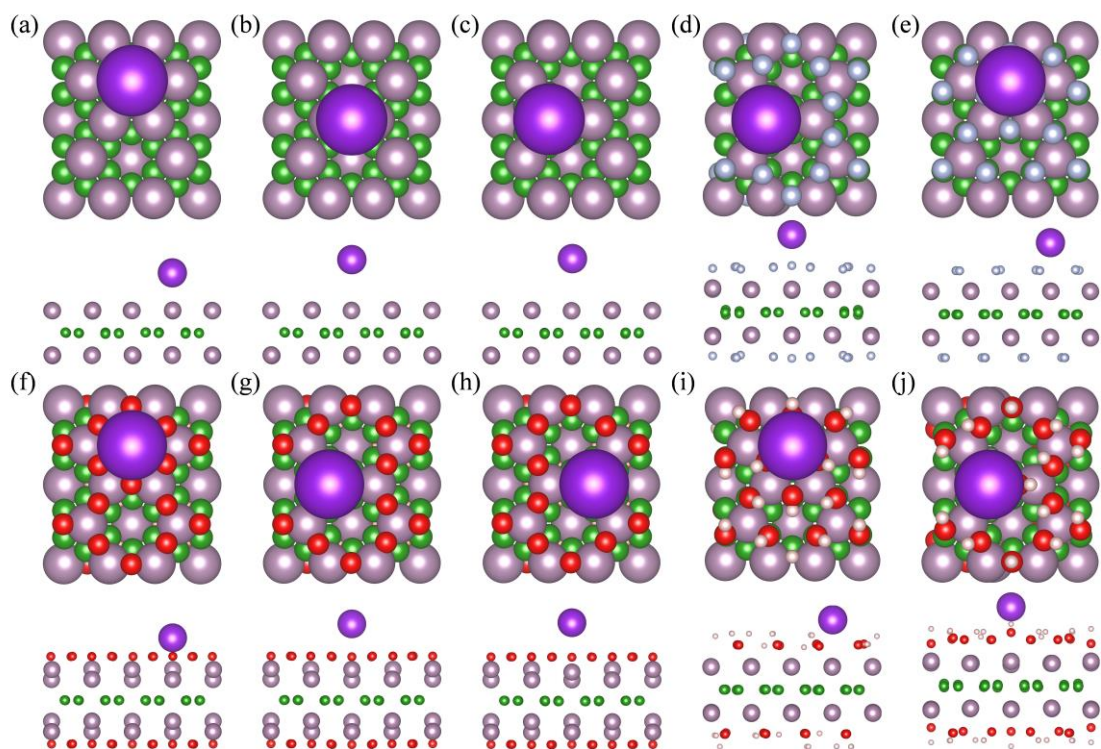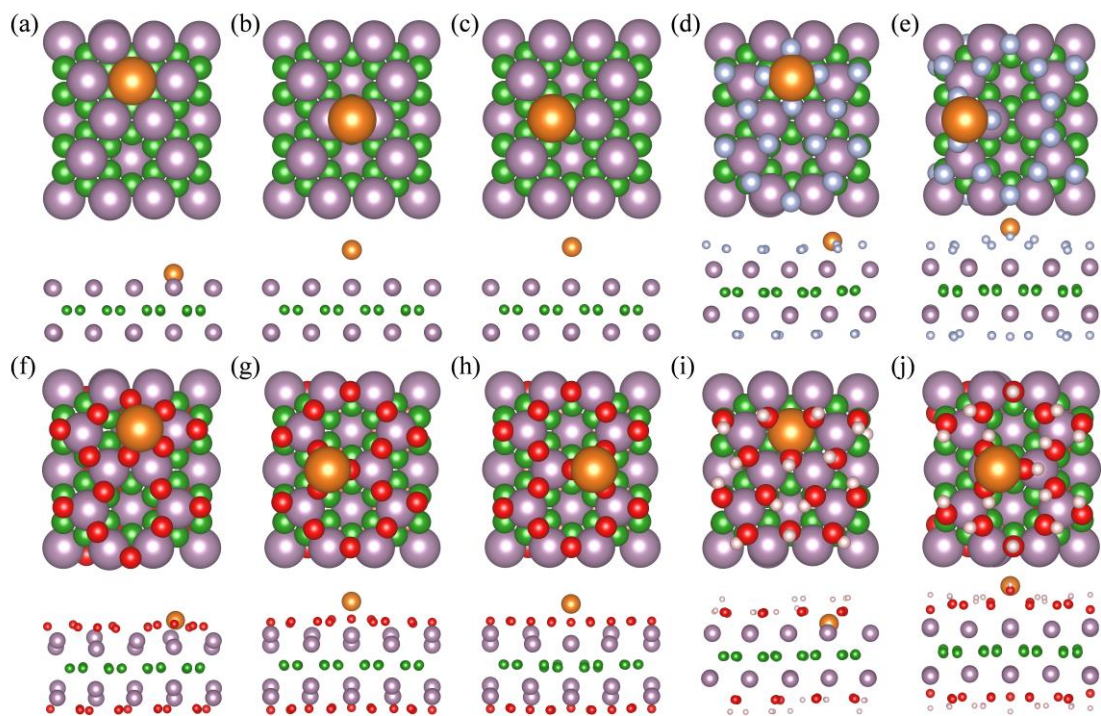Fig S3 Optimization results of F-termination adsorption sites: (a): hollow site; (b): bridge site and (c): top site.

Fig S4 Optimization results of Li ion adsorption sites: bare $Mo_{4/3}B_2$: (a): hollow site; (b): bridge site and (c): top site; $Mo_{4/3}B_2F_2$: (d): hollow site and (e): top site; $Mo_{4/3}B_2O_2$: (f): hollow site; (g): top-a site and (h): top-b site and $Mo_{4/3}B_2(OH)_2$: (i): hollow site and (j): top site.
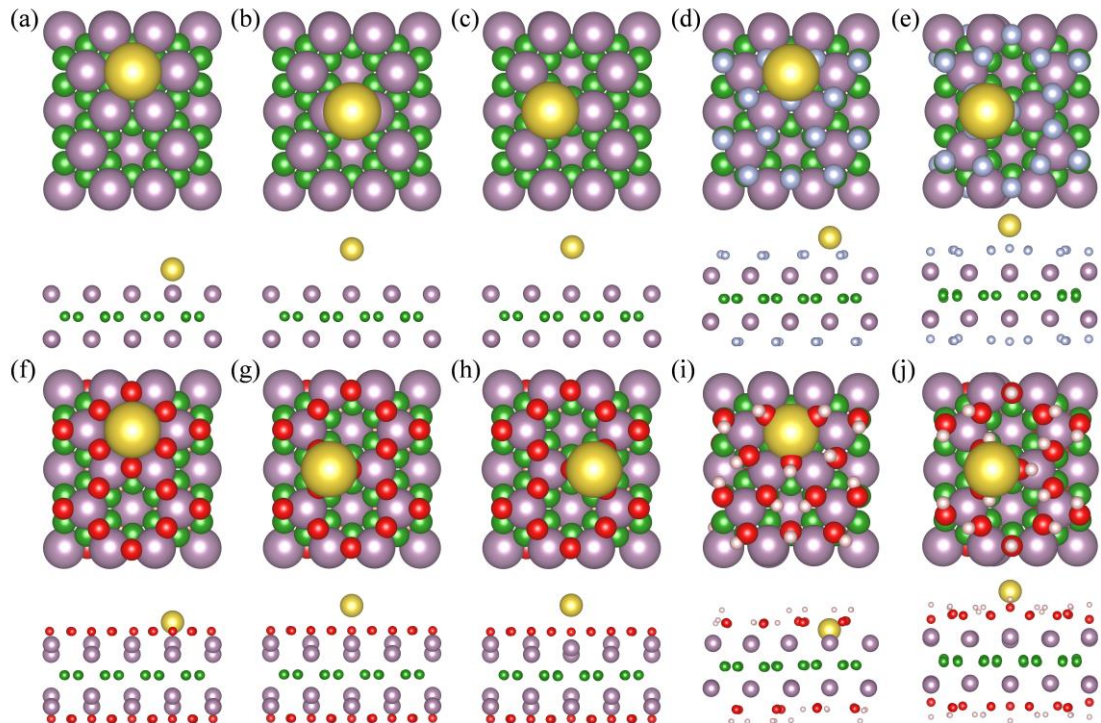
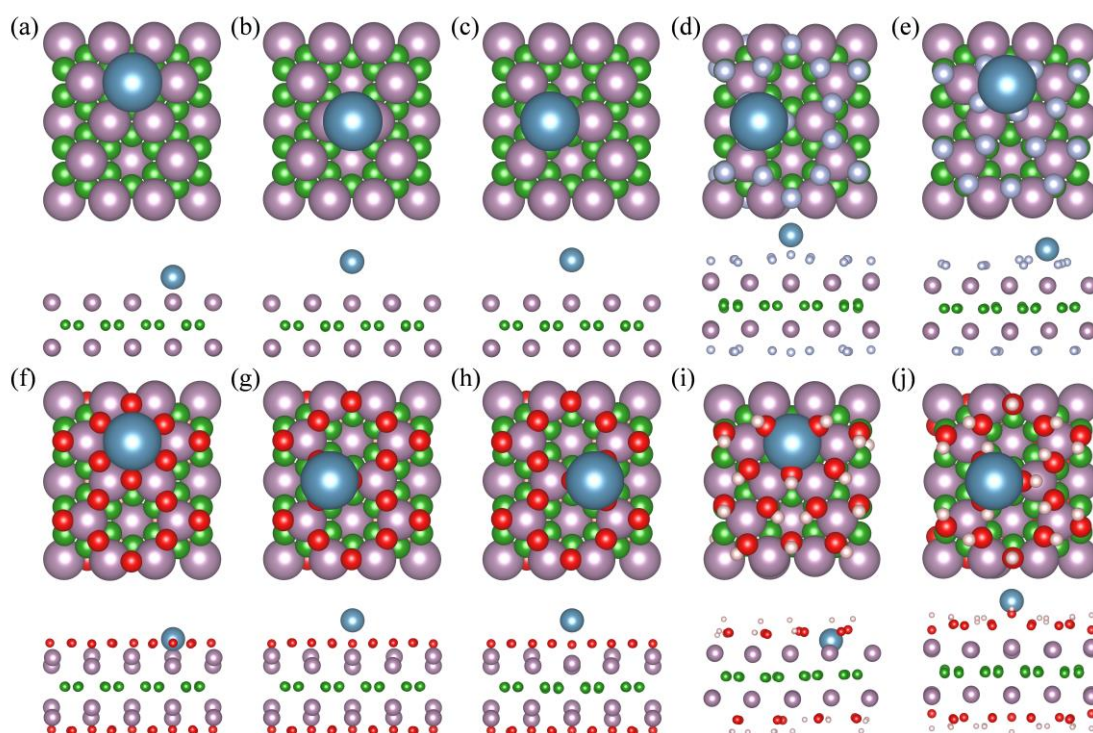Fig S5 Optimization results of Na ion adsorption sites: bare $Mo_{4/3}B_2$: (a): hollow site; (b): bridge site and (c): top site; $Mo_{4/3}B_2F_2$: (d): hollow site and (e): top site; $Mo_{4/3}B_2O_2$: (f): hollow site; (g): top-a site and (h): top-b site and $Mo_{4/3}B_2(OH)_2$: (i): hollow site and (j): top site.

Fig S6 Optimization results of K ion adsorption sites: bare $Mo_{4/3}B_2$: (a): hollow site; (b): bridge site and (c): top site; $Mo_{4/3}B_2F_2$: (d): hollow site and (e): top site; $Mo_{4/3}B_2O_2$: (f): hollow site; (g): top-a site and (h): top-b site and $Mo_{4/3}B_2(OH)_2$: (i): hollow site and (j): top site.

Fig S7 Optimization results of Mg ion adsorption sites: bare $Mo_{4/3}B_2$: (a): hollow site; (b): bridge site and (c): top site; $Mo_{4/3}B_2F_2$: (d): hollow site and (e): top site; $Mo_{4/3}B_2O_2$: (f): hollow site; (g): top-a site and (h): top-b site and $Mo_{4/3}B_2(OH)_2$: (i): hollow site and (j): top site.

Fig S8 Optimization results of Ca ion adsorption sites: bare $Mo_{4/3}B_2$: (a): hollow site; (b): bridge site and (c): top site; $Mo_{4/3}B_2F_2$: (d): hollow site and (e): top site; $Mo_{4/3}B_2O_2$: (f): hollow site; (g): top-a site and (h): top-b site and $Mo_{4/3}B_2(OH)_2$: (i): hollow site and (j): top site.
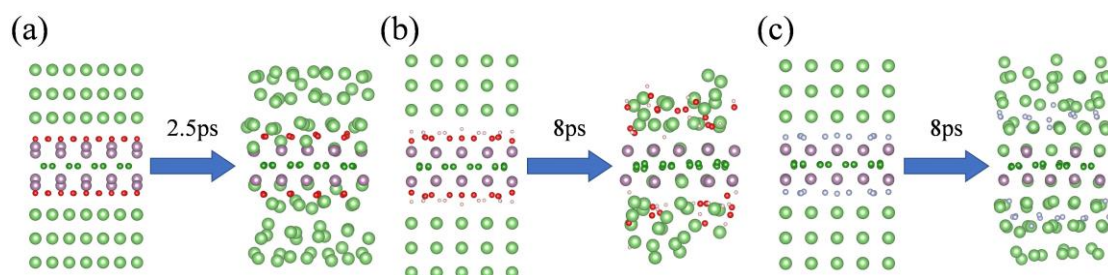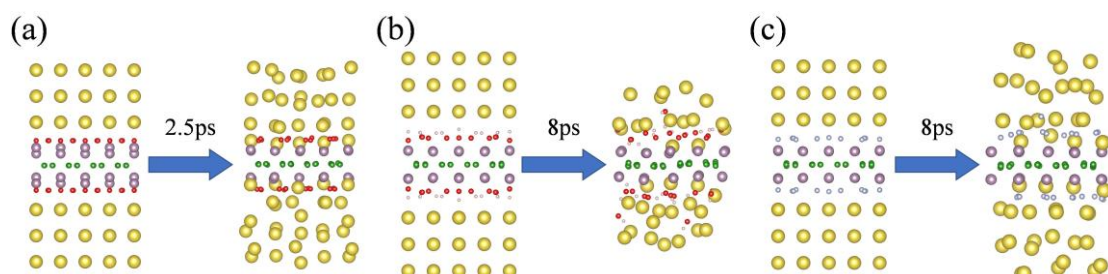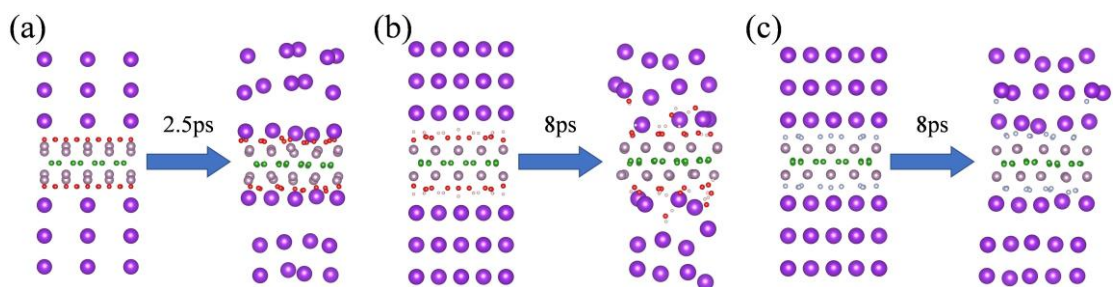

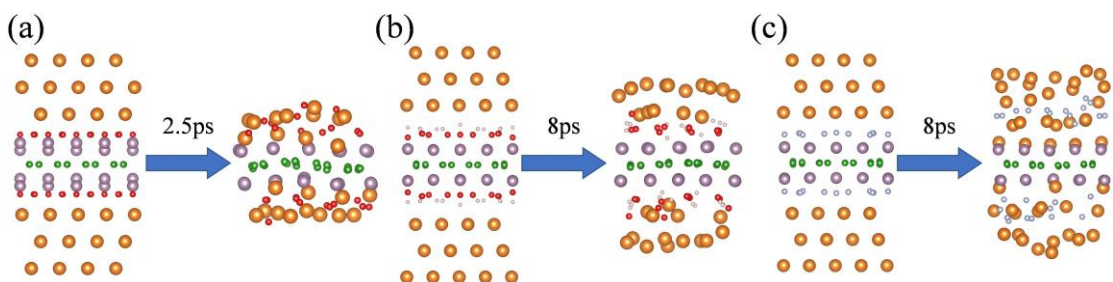Fig S9 Structural evolutions of Li-$Mo_{4/3}B_2T_2$-Li sandwich-like heterostructures simulated by FPMD at 300K within the NVT ensemble: (a) $Mo_{4/3}B_2O_2$; (b) $Mo_{4/3}B_2(OH)_2$; and (c) $Mo_{4/3}B_2F_2$.

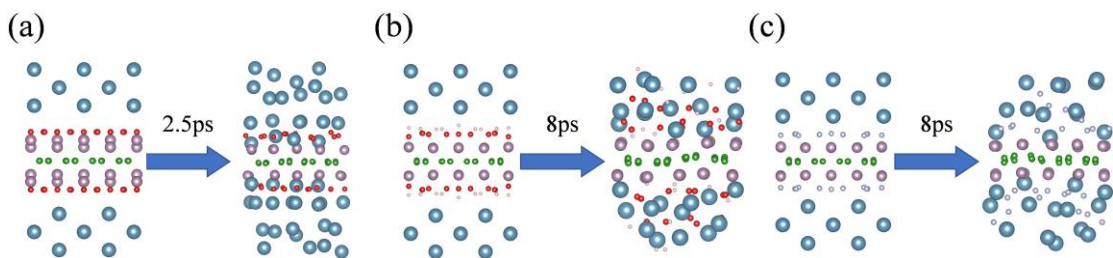

Fig S10 Structural evolutions of Na-$Mo_{4/3}B_2$-Na sandwich-like heterostructures simulated by FPMD at 300K within the NVT ensemble: (a) $Mo_{4/3}B_2O_2$; (b) $Mo_{4/3}B_2(OH)_2$; and (c) $Mo_{4/3}B_2F_2$.

Fig S11 Structural evolutions of K-Mo$_{4/3}$B$_2$-K sandwich-like heterostructures simulated by FPMD at 300K within the NVT ensemble: (a) Mo$_{4/3}$B$_2$O$_2$; (b) Mo$_{4/3}$B$_2$(OH)$_2$; and (c) Mo$_{4/3}$B$_2$F$_2$.

Fig S12 Structural evolutions of Mg-Mo$_{4/3}$B$_2$-Mg sandwich-like heterostructures simulated by FPMD at 300K within the NVT ensemble: (a) Mo$_{4/3}$B$_2$O$_2$; (b) Mo$_{4/3}$B$_2$(OH)$_2$; and (c) Mo$_{4/3}$B$_2$F$_2$.

Fig S13 Structural evolutions of Ca-Mo$_{4/3}$B$_2$-Ca sandwich-like heterostructures simulated by FPMD at 300K within the NVT ensemble: (a) Mo$_{4/3}$B$_2$O$_2$; (b) Mo$_{4/3}$B$_2$(OH)$_2$; and (c) Mo$_{4/3}$B$_2$F$_2$.
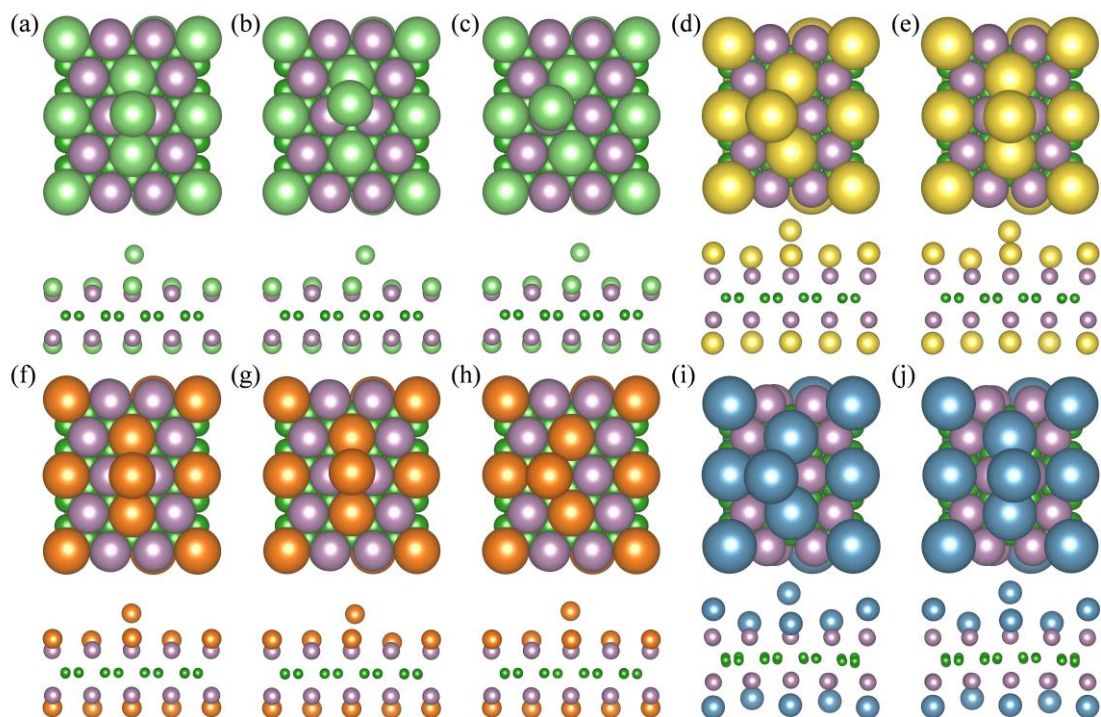
Fig S14 Optimization results of single ion adsorption sites in the second layer on $Mo_{4/3}B_2$: Li: (a): bridge site; (b): hollow site and (c): top site; Na: (d): top site and (e): bridge site; Mg: (f): bridge site; (g): hollow site and (h): top site and Ca: (i): top site and (j): bridge site.
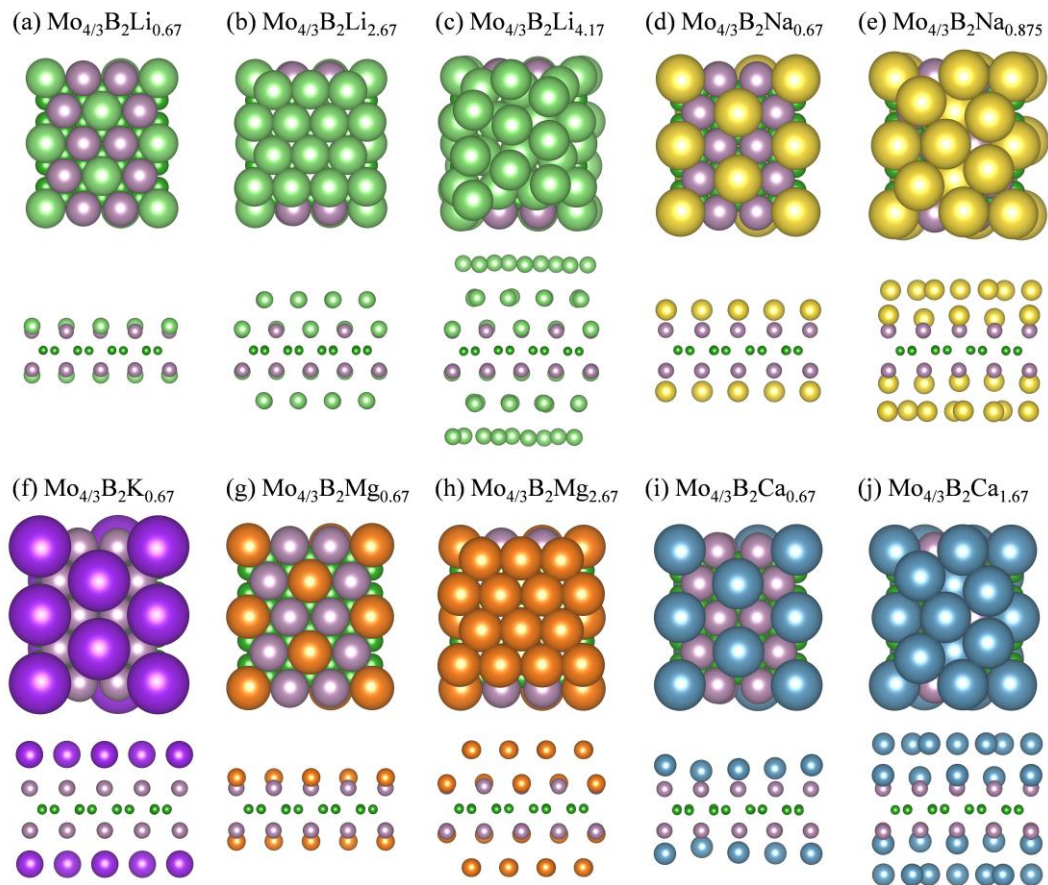
(a) $Mo_{4/3}B_2Li_{0.67}$ (b) $Mo_{4/3}B_2Li_{2.67}$ (c) $Mo_{4/3}B_2Li_{4.17}$ (d) $Mo_{4/3}B_2Na_{0.67}$ (e) $Mo_{4/3}B_2Na_{0.875}$

(f) $Mo_{4/3}B_2K_{0.67}$ (g) $Mo_{4/3}B_2Mg_{0.67}$ (h) $Mo_{4/3}B_2Mg_{2.67}$ (i) $Mo_{4/3}B_2Ca_{0.67}$ (j) $Mo_{4/3}B_2Ca_{1.67}$

Fig S15 (a) Top and side views of the structures of $Mo_{4/3}B_2Li_{0.67}$, (b) $Mo_{4/3}B_2Li_{2.67}$, (c) $Mo_{4/3}B_2Li_{4.17}$, (d) $Mo_{4/3}B_2Na_{0.67}$, (e) $Mo_{4/3}B_2Na_{0.875}$, (f) $Mo_{4/3}B_2K_{0.67}$, (g) $Mo_{4/3}B_2Mg_{0.67}$, (h) $Mo_{4/3}B_2Mg_{2.67}$, (i) $Mo_{4/3}B_2Ca_{0.67}$, and (j) $Mo_{4/3}B_2Ca_{1.67}$ with layers of Li/Na/K/Mg/Ca ions adsorbed on the 2D Boridene monolayer.
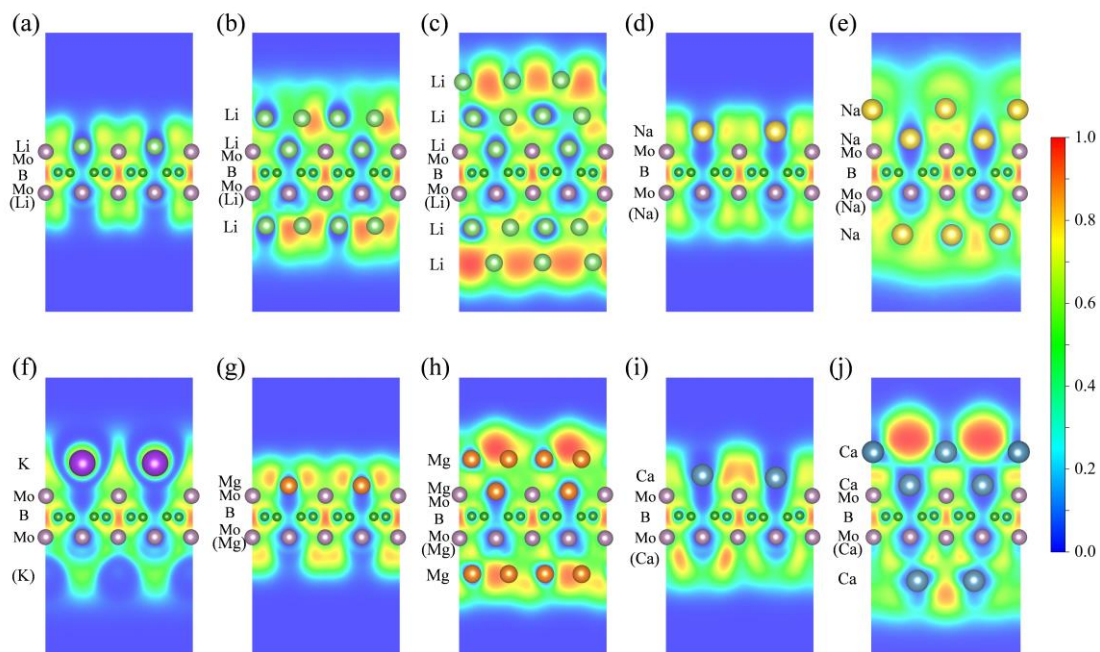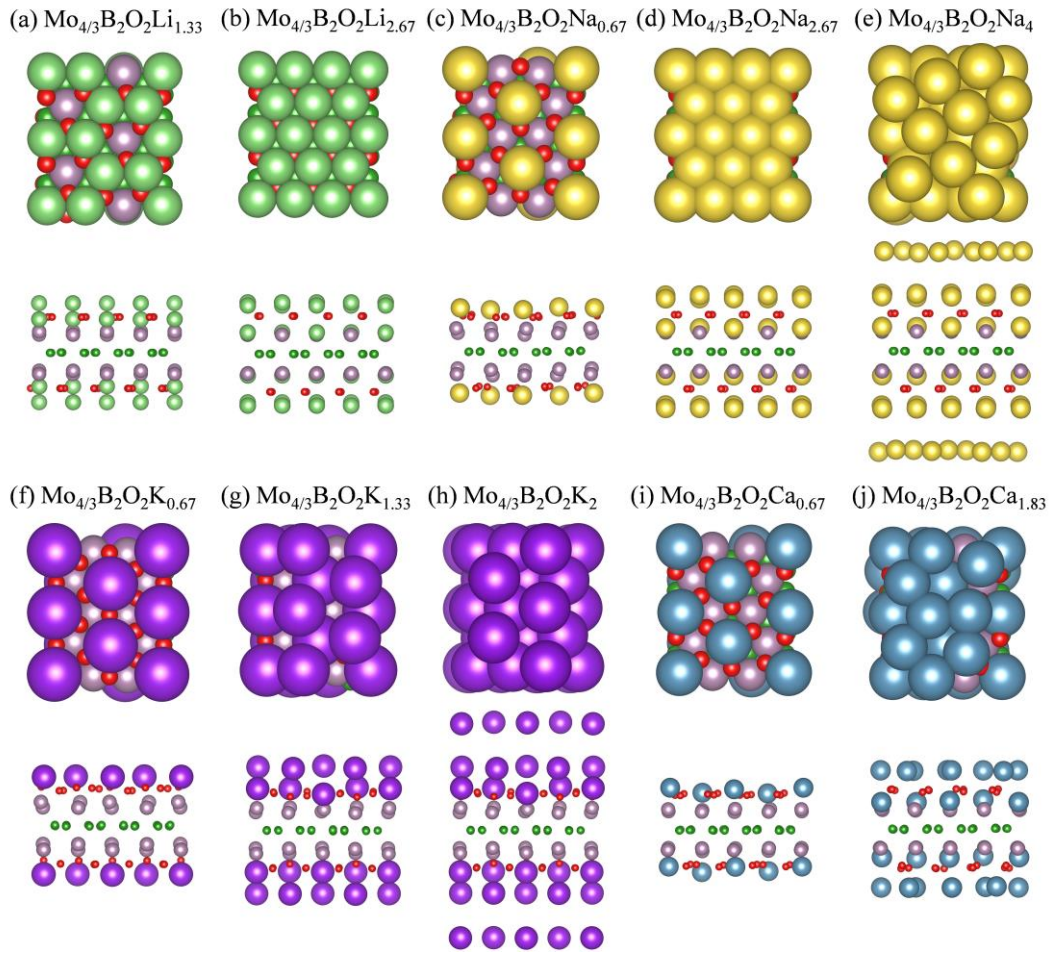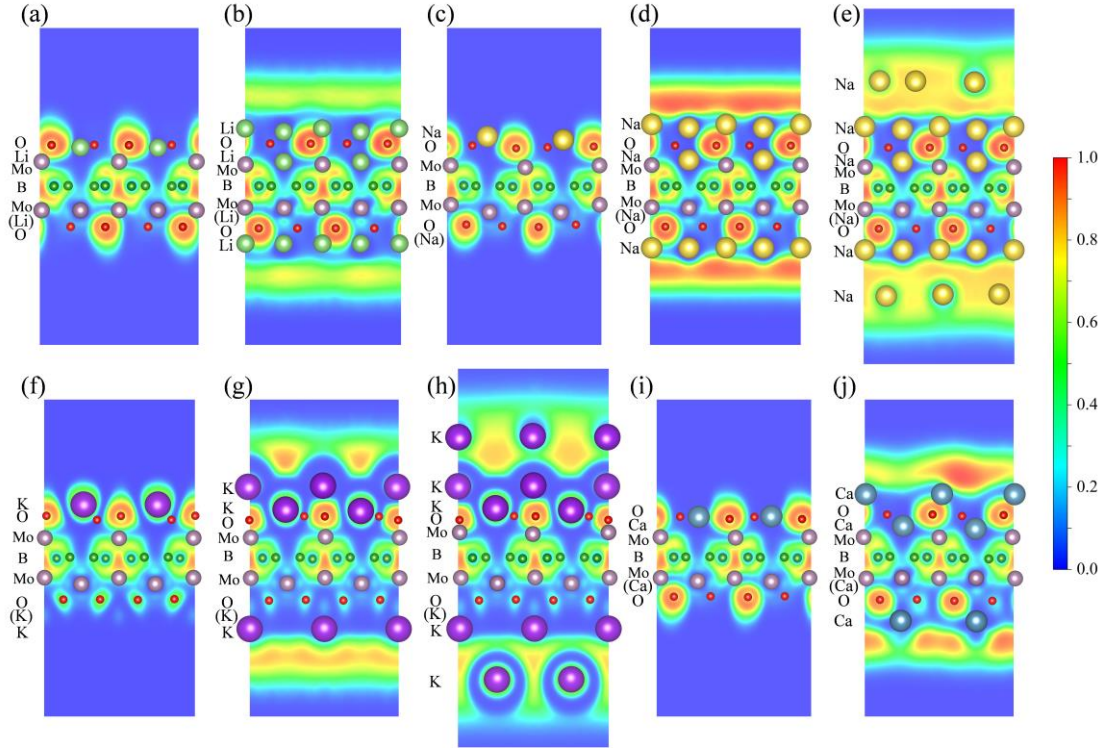

Fig S16 The 2-D contour plots of the electron localization function (ELF) of metal-ion saturated Boridene on (1 0 0) crystal plane: (a) $Mo_{4/3}B_2Li_{0.67}$, (b) $Mo_{4/3}B_2Li_{2.67}$, (c) $Mo_{4/3}B_2Li_{4.17}$, (d) $Mo_{4/3}B_2Na_{0.67}$, (e) $Mo_{4/3}B_2Na_{0.875}$, (f) $Mo_{4/3}B_2K_{0.67}$, (g) $Mo_{4/3}B_2Mg_{0.67}$, (h) $Mo_{4/3}B_2Mg_{2.67}$, (i) $Mo_{4/3}B_2Ca_{0.67}$, and (j) $Mo_{4/3}B_2Ca_{1.67}$ with layers of Li/Na/K/Mg/Ca ions adsorbed on the 2D Boridene monolayer.

(a) $Mo_{4/3}B_2O_2Li_{1.33}$ (b) $Mo_{4/3}B_2O_2Li_{2.67}$ (c) $Mo_{4/3}B_2O_2Na_{0.67}$ (d) $Mo_{4/3}B_2O_2Na_{2.67}$ (e) $Mo_{4/3}B_2O_2Na_4$

(f) $Mo_{4/3}B_2O_2K_{0.67}$ (g) $Mo_{4/3}B_2O_2K_{1.33}$ (h) $Mo_{4/3}B_2O_2K_2$ (i) $Mo_{4/3}B_2O_2Ca_{0.67}$ (j) $Mo_{4/3}B_2O_2Ca_{1.83}$

Fig S17 (a) Top and side views of the structures of $Mo_{4/3}B_2O_2Li_{1.33}$, (b) $Mo_{4/3}B_2O_2Li_{2.67}$, (c) $Mo_{4/3}B_2O_2Na_{0.67}$, (d) $Mo_{4/3}B_2O_2Na_{2.67}$, (e) $Mo_{4/3}B_2O_2Na_4$, (f) $Mo_{4/3}B_2O_2K_{0.67}$, (g) $Mo_{4/3}B_2O_2K_{1.33}$, (h) $Mo_{4/3}B_2O_2K_2$, (i) $Mo_{4/3}B_2O_2Ca_{0.67}$, and (j) $Mo_{4/3}B_2O_2Ca_{1.83}$ with layers of Li/Na/K/Ca ions adsorbed on the 2D $Mo_{4/3}B_2O_2$ monolayer.

Fig S18 The 2-D contour plots of the electron localization function (ELF) of metal-ion saturated Boridene on (1 0 0) crystal plane: (a) $Mo_{4/3}B_2O_2Li_{1.33}$, (b) $Mo_{4/3}B_2O_2Li_{2.67}$, (c) $Mo_{4/3}B_2O_2Na_{0.67}$, (d) $Mo_{4/3}B_2O_2Na_{2.67}$, (e) $Mo_{4/3}B_2O_2Na_4$, (f) $Mo_{4/3}B_2O_2K_{0.67}$, (g) $Mo_{4/3}B_2O_2K_{1.33}$, (h) $Mo_{4/3}B_2O_2K_2$, (i) $Mo_{4/3}B_2O_2Ca_{0.67}$, and (j) $Mo_{4/3}B_2O_2Ca_{1.83}$ with layers of Li/Na/K/Ca ions adsorbed on the 2D $Mo_{4/3}B_2O_2$ monolayer.

Fig S19 electronic density of states (DOS) for (a): $Mo_{4/3}B_2Li_{4.17}$; (b) $Mo_{4/3}B_2Na_{0.875}$; (C) $Mo_{4/3}B_2Mg_{2.67}$; (d) $Mo_{4/3}B_2Ca_{1.67}$; (e) $Mo_{4/3}B_2O_2Li_{2.67}$; (f) $Mo_{4/3}B_2O_2Na_4$; (g) $Mo_{4/3}B_2O_2K_2$; (h) $Mo_{4/3}B_2O_2Ca_{1.83}$.

S11
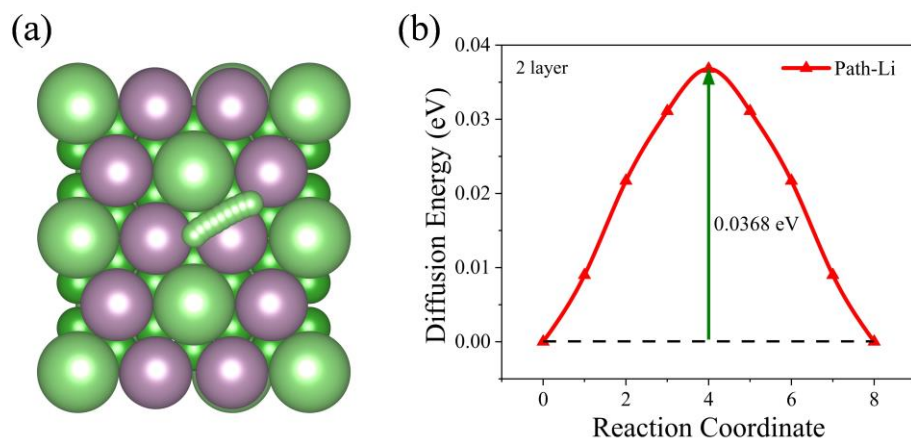
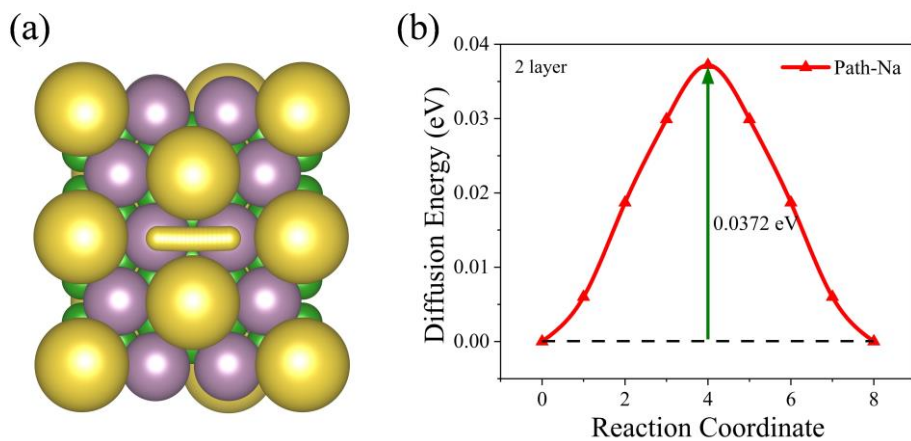Fig S20 The proposed migration pathway and diffusion energy profile of Li ion in the second layer on $Mo_{4/3}B_2$

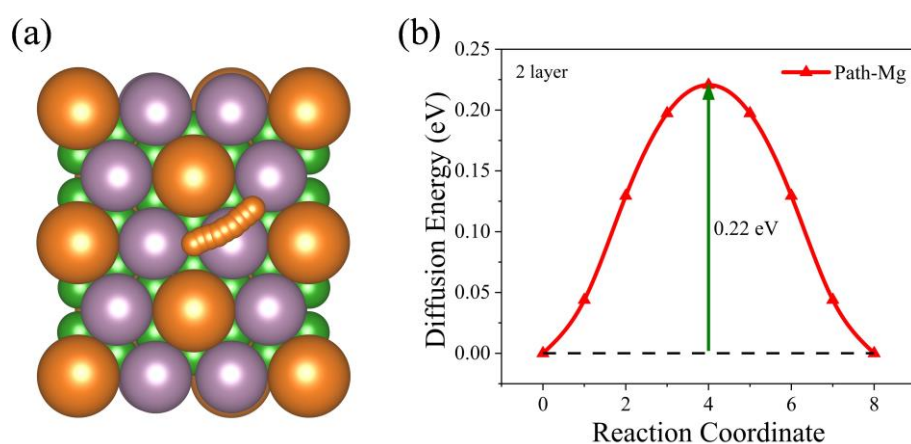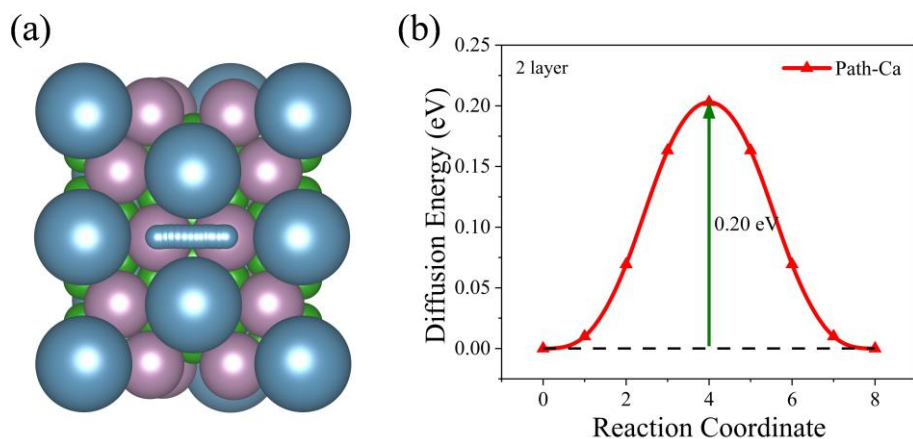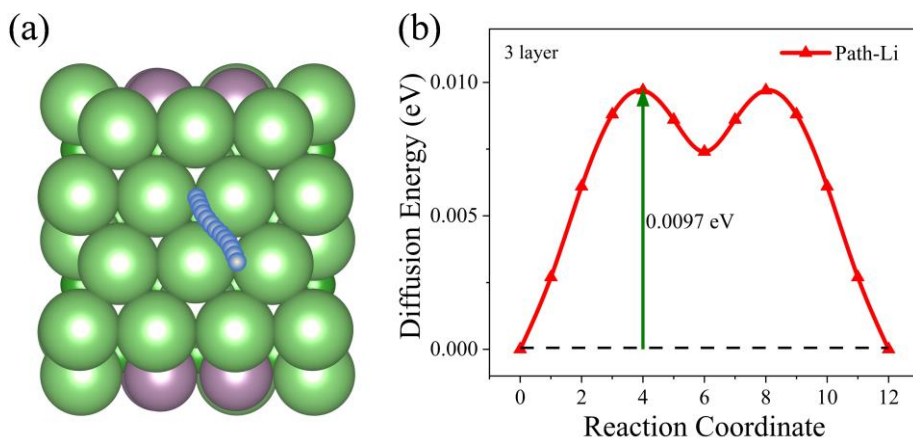Fig S21 The proposed migration pathway and diffusion energy profile of Na ion in the second layer on $Mo_{4/3}B_2$

Fig S22 The proposed migration pathway and diffusion energy profile of Mg ion in the second layer on $Mo_{4/3}B_2$

Fig S23 The proposed migration pathway and diffusion energy profile of Ca ion in the second layer on $Mo_{4/3}B_2$

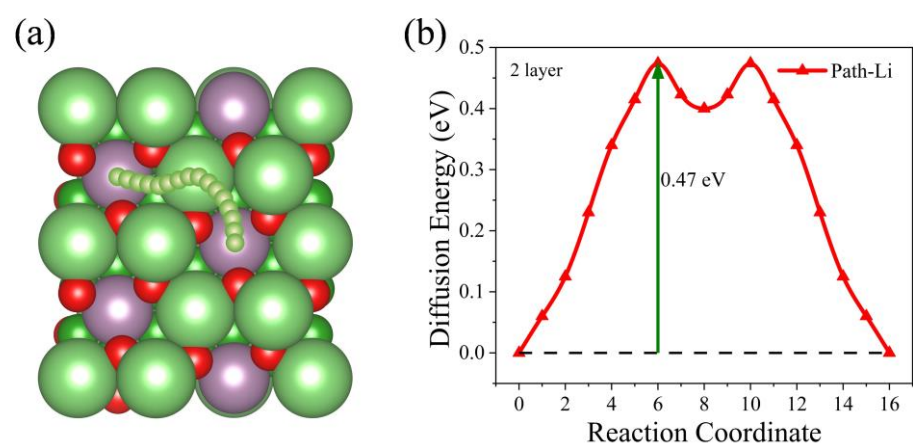Fig S24 The proposed migration pathway and diffusion energy profile of Li ion in the third layer on $Mo_{4/3}B_2$

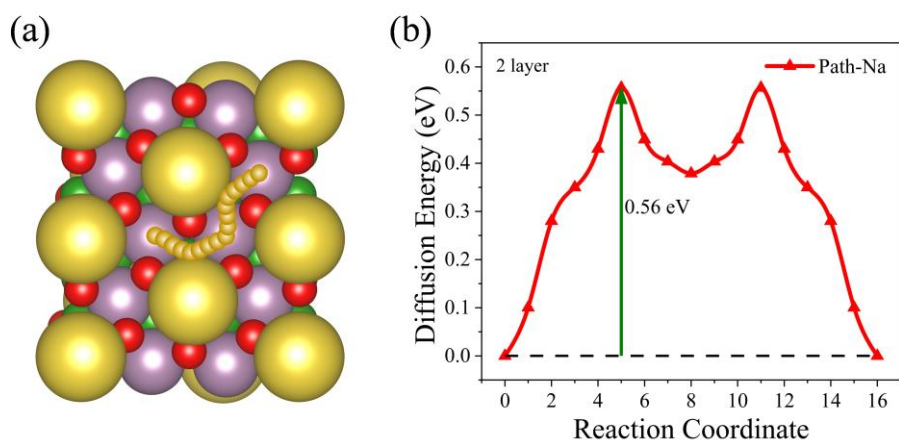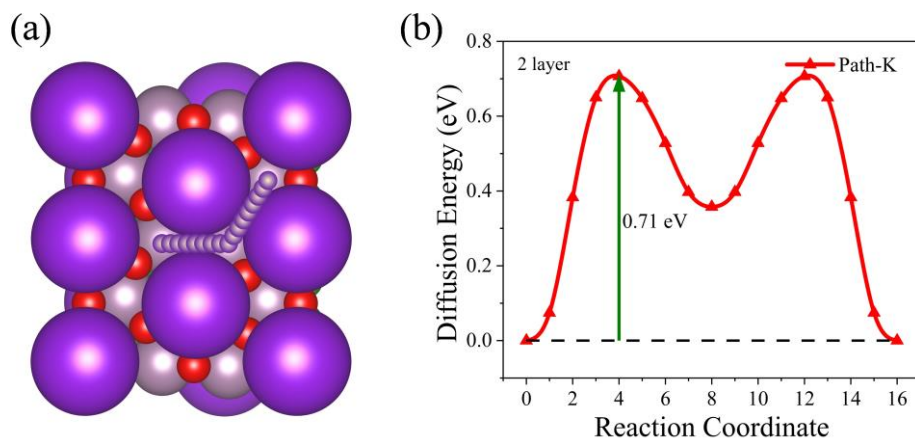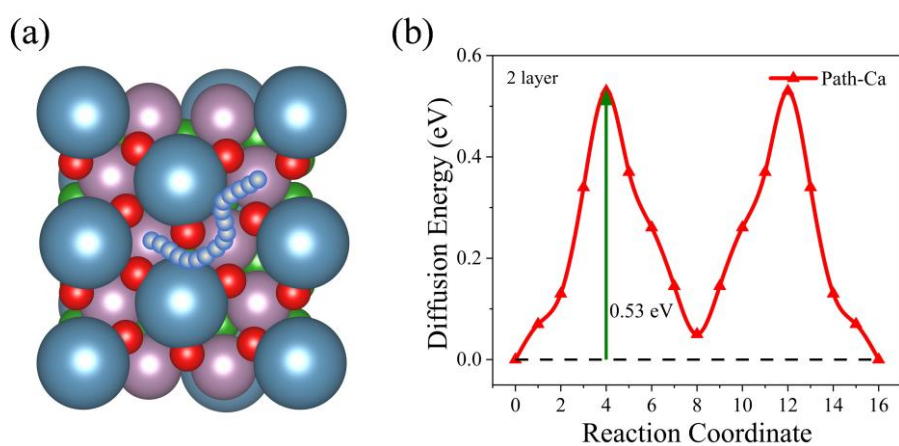Fig S25 The proposed migration pathway and diffusion energy profile of Li ion in the second layer on $Mo_{4/3}B_2O_2$

Fig S26 The proposed migration pathway and diffusion energy profile of Na ion in the second layer on $Mo_{4/3}B_2O_2$

Fig S27 The proposed migration pathway and diffusion energy profile of K ion in the second layer on $Mo_{4/3}B_2O_2$

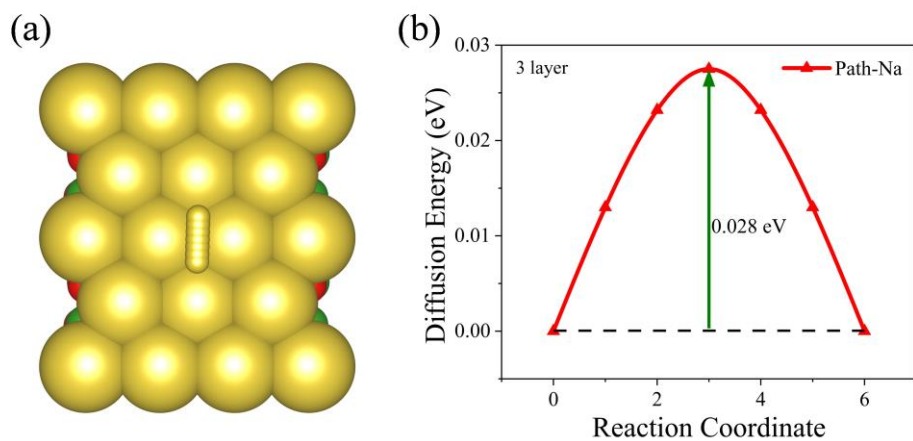Fig S28 The proposed migration pathway and diffusion energy profile of Ca ion in the second layer on $Mo_{4/3}B_2O_2$

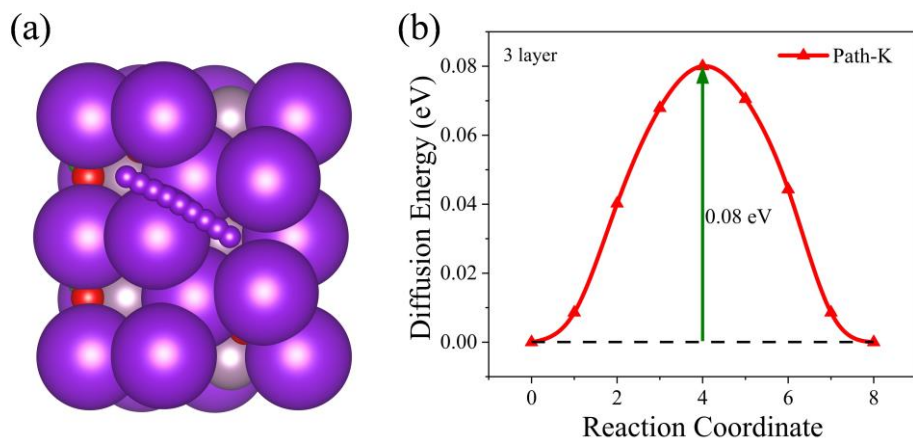Fig S29 The proposed migration pathway and diffusion energy profile of Na ion in the third layer on $Mo_{4/3}B_2O_2$

Fig S30 The proposed migration pathway and diffusion energy profile of K ion in the third layer on $Mo_{4/3}B_2O_2$